ISSN 0869-5911, Petrology, 2021, Vol. 29, No. 4, pp. 439–447. © Pleiades Publishing, Ltd., 2021.

Phase State and Thermodynamic Parameters of the Fluid System H_2O–CO_2–CH_4 at *P-T* Conditions of the Crust and Lithosphere Mantle

M. V. Ivanov[a], * and O. V. Alexandrovich[a]

[a] *Institute of Precambrian Geology and Geochronology, Russian Academy of Sciences, St. Petersburg, Russia*

**e-mail: m.v.ivanov@ipgg.ru*

Received January 26, 2021; revised February 12, 2021; accepted March 29, 2021

Abstract—Calculations of the thermodynamic properties of the ternary fluid system H_2O–CO_2–CH_4 in a broad range of *P-T* parameters above the critical point of water are presented. The calculations are based on the known equations of state for binary systems H_2O–CO_2 and H_2O–CH_4, which were extended up to equation of state of the ternary system by means of the Lorentz–Berthelot mixing rules. The obtained equation for the Gibbs excess free energy allows determining the phase state of the system (homogeneous of two-phase fluid) and obtaining chemical activities of components, densities and compressibility of fluid phases, as well as other thermodynamic properties of the fluid. The equations and methods of calculations can be applied in the range of *P-T* parameters of $P = 0.1$–100 kbar and $T = 400$–2300°C, i.e. in the range from metamorphic processes of the greenschist facie up to deep layers of the lithosphere mantle. We obtained phase diagrams of the system H_2O–CO_2–CH_4 and investigated dependencies of the chemical activity of water on concentrations of the components and temperature and pressure. The conditions for splitting of the fluid into co-existing immiscible phases are investigated in detail. The splitting in the system H_2O–CO_2–CH_4 appears to be possible in the temperature range from 400 up to 735°C. In the range of temperatures 400–480°C and pressures 1.1–10 kbar broad fields of co-existing phases are present on phase diagrams. For the three binary boundary subsystems, the splitting at these *P-T* conditions is possible only in the system H_2O–CH_4. Nevertheless, the presence of methane in the ternary system enables the emergence of immiscible fluid phases with high concentration of CO_2, which could exceed the concentration of the methane. At temperatures above 500°C the phase behavior of the system H_2O–CO_2–CH_4 is similar to the behavior of the majority of salt-free gas-water fluids, i.e. the splitting into two immiscible phases occurs at high pressures, corresponding to *P-T* conditions of the cold subduction.

Keywords: crust, lithosphere mantle, fluid system H_2O–CO_2–CH_4, salt-free fluid, phase state, density of the fluid, composition and activity of components

DOI: 10.1134/S0869591121040032

INTRODUCTION

Carbon dioxide and methane are widespread components of gas, gas-water, and gas-water-salt fluids contained in mineral microinclusions of rocks of various composition, age, and *P-T* conditions of formation (Fonarev and Kreulen, 1995; Fonarev et al., 1998; Liebscher and Heinrich, 2007; Liebscher, 2007; Aranovich, 2013; Manning and Aranovich, 2014; Manning, 2018; Bushmin et al., 2020). The main direction in the thermodynamic modeling of three-component fluid systems for *P-T* conditions above the critical point of water is the study of the phase state and possibility of phase splitting of a fluid, containing one of the gases, common in natural fluids and an aqueous solution of a salt, such as an alkali or alkaline earth metal chloride (Duan et al., 1995; Joyce and Holloway, 1993; Aranovich et al., 2010; Ivanov and Bushmin, 2019, 2021). It is well known that the presence of a dissolved salt in a fluid greatly facilitates its splitting into conditionally gaseous and conditionally liquid phases. Therefore, such a choice of theoretically studied systems is a logical step towards modelling the thermodynamic behavior of natural fluids, which, as a rule, have a much more complex composition. Systems of several neutral gases and water are widespread in nature, and modern methods for studying fluid inclusions, primarily Raman spectroscopy (Frezzotti et al., 2012), make it possible to quantitatively determine the content of water and various gases in fluid inclusions. An exception with a model for a fluid, containing two gases, is the work (Zhao, 2017), in which the system H_2O–CO_2–CH_4 is studied in detail for temperatures below the critical point of water.

The aim of this work is to study the phase behavior of the H_2O–CO_2–CH_4 ternary system in a wide range of *P-T* conditions above the critical point of water and

obtaining thermodynamic parameters of such a fluid, important from a geological point of view, primarily the phase state of the fluid, the chemical activity of water, and density of fluid phases.

METHOD

In (Zhang and Duan, 2009), an equation of state for water and several non-polar gases was obtained. This equation also allows generalization for mixtures of these substances. A significant advantage of the equation (Zhang and Duan, 2009) is a very wide range of *P-T* conditions, in which this equation reproduces with high accuracy the experimental data and the results of theoretical calculations using the molecular dynamics (MD) method. For three pure substances H_2O, CO_2, and CH_4, as well as binary systems H_2O–CO_2 and H_2O–CH_4, the admissible temperatures and pressures cover the range $0.1 \le P \le 100$ kbar and $400 \le T \le 2300$°C. The equation of state by (Zhang and Duan, 2009) looks like:

$$Z = \frac{P_m V_m}{RT_m} = 1 + \frac{a_1 + a_2/T_m^2 + a_3/T_m^3}{V_m} + \frac{a_4 + a_5/T_m^2 + a_6/T_m^3}{V_m^2} + \frac{a_7 + a_8/T_m^2 + a_9/T_m^3}{V_m^4} + \frac{a_{10} + a_{11}/T_m^2 + a_{12}/T_m^3}{V_m^5} + \frac{a_{13}}{T_m^3 V_m^2}\left(a_{14} + \frac{a_{15}}{V_m^2}\right)\exp\left(-\frac{a_{15}}{V_m^2}\right). \quad (1)$$

Here Z is the compressibility coefficient, $R = 8.3144626$ J/K/mol is the universal gas constant, P_m, V_m and T_m are modified values of pressure, molar volume, and absolute temperature. These modified values are expressed in terms of the corresponding values P, V, and T in SI units (Pa, m^3, K) as follows:

$$P_m = \frac{3.063\sigma^3}{\varepsilon} \times 10^{-3} P; \quad V_m = \left(\frac{3.691}{\sigma}\right)^3 \times 10^3 V; \quad T_m = \frac{154}{\varepsilon} T. \quad (2)$$

It is easy to verify that, when substituted into the formula for the compressibility coefficient, the numerical factors in expressions (3) cancel out, and the quantity Z takes its usual form:

$$Z = \frac{PV}{RT}.$$

The parameters a_1, ..., a_{15} are common for all the molecules considered by (Zhang and Duan, 2009). The Lenard–Jones parameters ε (the usual way of specifying this quantity is ε/k_B with dimensions in Kelvins) and σ [Å] are individual for each pure substance (Zhang and Duan, 2009). For mixtures they are calculated according to the Lorentz–Berthelot mixing rules:

$$\varepsilon = \sum_{i=1}^{n}\sum_{j=1}^{n} x_i x_j k_{1,ij}\sqrt{\varepsilon_i \varepsilon_j}, \quad (3a)$$

$$\sigma = \sum_{i=1}^{n}\sum_{j=1}^{n} x_i x_j k_{2,ij}(\sigma_i + \sigma_j)/2, \quad (3b)$$

where n is the number of components in the mixture; x_i is the mole fraction of component i; ε_i and σ_i are Lenard–Jones parameters for the corresponding component. The values of the parameters a_1, ..., a_{15}, ε_i and σ_i are given in (Zhang and Duan, 2009). The individual properties of the binary interaction of components are set by the values of the parameters $k_{1,ij}$ and $k_{2,ij}$. The matrices $\mathbf{k}_1$ and $\mathbf{k}_2$ are symmetric, and $k_{1,ii} = k_{2,ii} = 1$.

The numerical values of the coefficients $k_{1,ij}$, $k_{2,ij}$ were obtained in (Zhang and Duan, 2009) for two binary subsystems of the ternary H_2O–CO_2–CH_4 system, namely H_2O–CO_2 and H_2O–CH_4, by fitting experimental and MD data on the *PVTx* properties of these binary systems. For the H_2O–CO_2 system, the optimal values $k_{1,12} = k_{1,21} = 0.85$ and $k_{2,12} = k_{2,21} = 1.02$ were obtained. The corresponding values for the H_2O–CH_4 system are $k_{1,12} = k_{1,21} = 0.8$ and $k_{2,12} = k_{2,21} = 1.0$. Also in (Zhang and Duan, 2009), the formulas of the thermodynamic model, for these two systems, were tested under the assumption that all the elements of the matrices $\mathbf{k}_1$ and $\mathbf{k}_2$ are equal to unity. For both systems, consisting of non-polar gas molecules and water molecules, having a significant dipole moment, only a minor decrease in the model accuracy was recorded. It is natural to assume that the electrostatic interaction of two molecules of non-polar gases will be weaker (in comparison with the Lenard–Jones interaction) than such interaction of a molecule of any of the gases CO_2 and CH_4 with a water molecule. Thus, this interaction will cause a smaller deviation of the coefficients $k_{1,ij}$, $k_{2,ij}$ from unity. As a consequence, the interaction in the binary system CO_2–CH_4 should be described quite accurately when using the values $k_{1,12} = k_{1,21} = 1$ and $k_{2,12} = k_{2,21} = 1$. This choice leads to the construction of a model of the H_2O–CO_2–CH_4 ternary system using formulas (1)–(3), (A2)–(A7) with matrices:

$$\mathbf{k}_1 = \begin{pmatrix} 1 & 0.85 & 0.8 \\ 0.85 & 1 & 1 \\ 0.8 & 1 & 1 \end{pmatrix} \text{ and } \mathbf{k}_2 = \begin{pmatrix} 1 & 1.02 & 1 \\ 1.02 & 1 & 1 \\ 1 & 1 & 1 \end{pmatrix}. \quad (4)$$

Hereinafter, the values of the indices for mole fractions are $x_1 = x_{H_2O}$, $x_2 = x_{CO_2}$, and $x_3 = x_{CH_4}$, and similarly for other quantities with indices.

To determine the phase state of a three-component system and calculate most of its thermodynamic

parameters, it is necessary, in addition to Eq. (1), to have expressions for the Gibbs free energy and/or for closely related quantities, such as activity or fugacity of components. The formulas for the fugacity of components presented in (Zhang and Duan, 2009) are published with major misprints, making direct using these formulas impossible. Correct thermodynamic formulas corresponding to Eq. (1) are derived in the Appendix.

In practical calculations for the ternary system H_2O–CO_2–CH_4, we carried out a numerical minimization of the molar free energy of the system, under the assumption that the system consists of two immiscible phases, *a* and *b:*

$$G_{\text{mix}} = y^a G^a_{\text{mix}}(x_1^a, x_2^a, x_3^a) + y^b G^b_{\text{mix}}(x_1^b, x_2^b, x_3^b), \quad (5)$$

where the quantities $y^a, y^b, x_1^a, x_2^a, x_3^a, x_1^b, x_2^b, x_3^b$ are bound by ratios that ensure the preservation of the given total composition of the system (x_1, x_2, x_3). The coincidence of the compositions of phases for the minimum possible value of G_{mix}, or the disappearance of one of the phases as a result of minimization, means the absence of phase splitting in the system.

RESULTS

The calculated phase diagrams of the H_2O–CO_2–CH_4 system in the coordinates of the molar fractions of H_2O, CO_2, and CH_4 are shown in Figs. 1–3. Phase diagrams for $T = 400$°C and nine pressure values from 1 to 20 kbar are presented in Fig. 1. The solvus, i.e., the boundary between the homogeneous fluid region (denoted by the number 1 in a box) and the heterogeneous fluid region (denoted by the number 2 in a box), is shown in the diagrams by the bold blue line.

At all the *P-T* conditions, when the fluid H_2O–CO_2–CH_4 can split into two coexisting immiscible phases, the splitting also occurs in the H_2O–CH_4 binary subsystem. Unlimited miscibility of water with gas in this system is possible only at significantly lower pressures than in the H_2O–CO_2 binary system. Consequently, the region of the heterogeneous fluid in all the cases touches the left side of the composition triangle. In addition to solvuses, isolines of the water activity in a homogeneous fluid (thin colored curves) are shown in the phase diagrams. The corresponding values of a_{H_2O} are also given in the figures. The points of intersection of the isolines of water activity with the solvus are ends of tie lines (dashed) connecting the points of the composition of the fluid phases coexisting in the heterogeneous region.

The region of heterogeneous fluid is present in all the phase diagrams of Fig. 1 starting from $P = 2$ kbar. The size of this area increases significantly with increasing pressure. It should be noted, that the region of the heterogeneous fluid increases not only due to falling the miscibility of water and methane with increasing pressure, but also due to an increase in the CO_2 content in the composition of the heterogeneous fluid. The phase diagrams for $P = 14$ kbar and $P = 20$ kbar reflect the possibility of the phase splitting in the binary subsystem H_2O–CO_2, which does not contain methane. However, even at lower pressures, coexisting fluid phases in a heterogeneous region can contain significantly more carbon dioxide than methane. An extreme example of this can be seen in the phase diagram for $T = 400$°C and $P = 12$ kbar. Tie line of water activity $a_{H_2O} = 0.9$ connects coexisting phases with compositions $x_{CO_2} = 0.20$, $x_{CH_4} = 0.025$ and $x_{CO_2} = 0.48$, $x_{CH_4} = 0.08$. That is, a minor content of methane enables the splitting of a predominantly aqueous-carbon dioxide fluid. In the absence of methane impurities in the system, such splitting into immiscible phases could not occur. At lower pressures, that is, in a more common geological situation, the presence of methane also allows for the coexistence of immiscible fluid phases with high CO_2 content.

As seen from Fig. 1, the region of coexistence of immiscible fluid phases in the H_2O–CO_2–CH_4 system is characterized by very high values of water activity about 0.9–0.95 and even higher values at pressures of 10–20 kbar. Isolines corresponding to lower water activities turn out to be bent and shifted to the region of relatively low water concentrations and high concentrations of CO_2 and CH_4. The same peculiar behavior of water activity isolines can be observed in the phase diagram for $T = 400$°C and $P = 1$ kbar, despite the fact that the field of a heterogeneous fluid is absent under these *P-T* conditions.

The temperature $T = 400$°C is the lower temperature limit for which the parameters of the equation of state (2) were reliable determined based on experimental data and calculations by the MD method (Zhang and Duan, 2009). In Figure 2, we show the phase diagrams of the H_2O–CO_2–CH_4 system at a higher temperature $T = 440$°C and pressure change from 4 to 30 kbar. Up to a shift towards higher pressures, the sequence of these phase diagrams demonstrates the same features and trends as the sequence for $T = 400$°C, Fig. 1. The most important result that follows from the phase diagrams in Figs. 1, 2 is the presence of significant areas of the composition of a salt-free fluid, in which it splits into immiscible phases at moderate pressures up to 8–10 kbar. The results presented in Figs. 1, 2 refer to temperatures 400 and 440°C. In Fig. 4, we present the temperature-dependent minimum pressures at which the phase splitting of the H_2O–CO_2 and H_2O–CH_4 binary fluids can occur. The splitting of the binary system H_2O-CH_4 at pressures up to 10 kbar can occur at $T \le 480$°C with the appearance of fields of a heterogeneous fluid in the phase diagrams of the H_2O–CO_2–CH_4 system, similar to those shown in Figs. 1, 2.

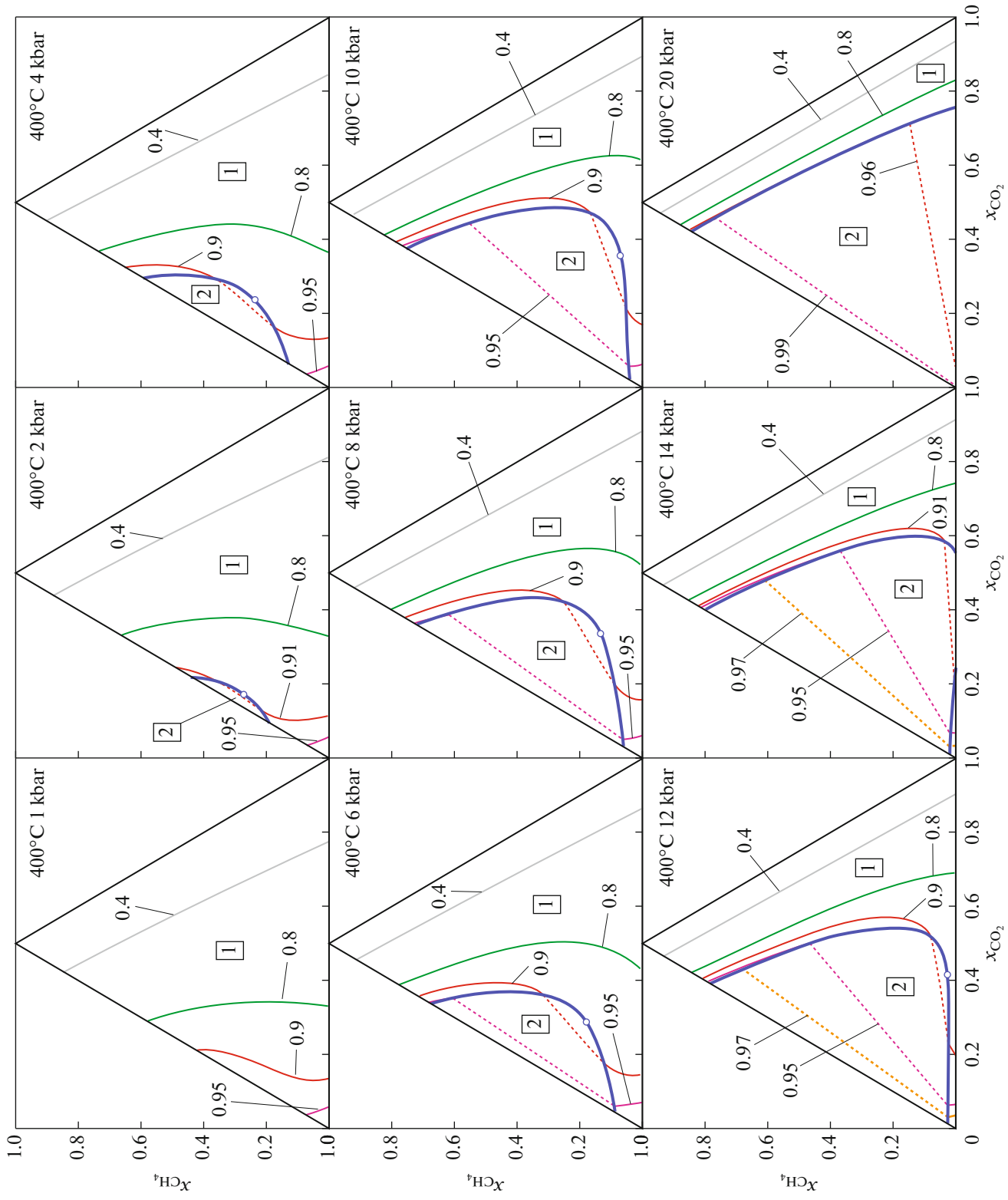

Fig. 1. Phase diagrams of the H_2O–CO_2–CH_4 ternary fluid system at $T = 400$°C and pressures from 1 to 20 kbar. The blue bold solid line is the boundary of the region of coexistence of two fluid phases (solvus). The numbers in the boxes indicate areas (fields) of different phase composition: homogeneous fluid—1; two coexisting fluid phases—2. Thin curves are isolines of water activity. Numbers with arrows indicate the values of a_{H_2O} corresponding to isolines. Dotted straight lines are the corresponding tie lines in areas of coexistence of two fluid phases. The open circles on the solvus indicate critical points corresponding to the minimum water activity in the area of coexistence of two fluid phases.

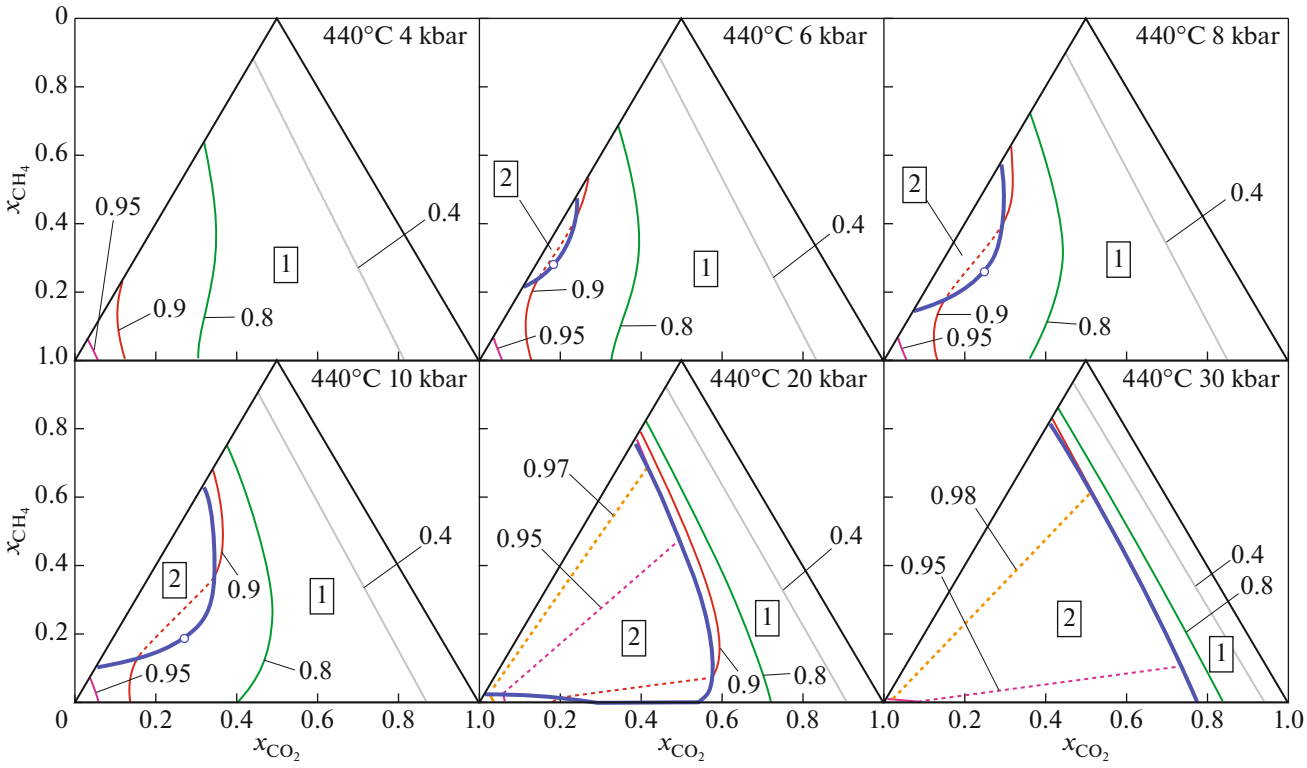

Fig. 2. Phase diagrams of the H_2O–CO_2–CH_4 ternary fluid system at $T = 440$°C and pressures from 4 to 30 kbar. Same notations as in Fig. 1.

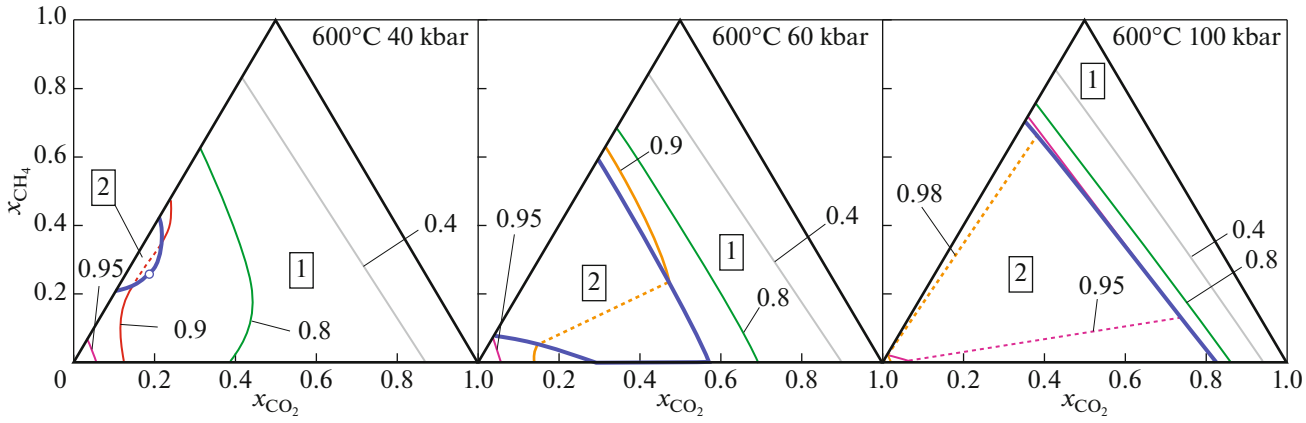

Fig. 3. Phase diagrams of the H_2O–CO_2–CH_4 ternary fluid system at $T = 600$°C and pressures from 40 to 100 kbar. Same notations as in Fig. 1.

At $T = 400$°C the appearance of a heterogeneous fluid is possible at $P \geq 1.1$ kbar (left border of the curve for H_2O–CH_4 in Fig. 4). In the H_2O–CO_2 system at $T = 400$°C the splitting is possible starting from $P = 13$ kbar. As the temperature rises, Fig. 4 shows the rapid increase in pressures required for the splitting of a homogeneous fluid into two phases. At the upper limit of the pressure range $P = 100$ kbar studied by us, the splitting of the H_2O–CO_2 binary fluid is possible at $T \leq 725$°C. For binary fluid H_2O–CH_4, the corresponding upper temperature limit is $T = 735$°C.

An example of the phase behavior of the H_2O–CO_2–CH_4 fluid system at temperature 600°C is given in Fig. 3. Qualitatively, the changes in the size and shape of the phase fields differ little from Figs. 1, 2. The pressures from 40 to 100 kbar, at which the phenomena of phase splitting are observed, correspond to

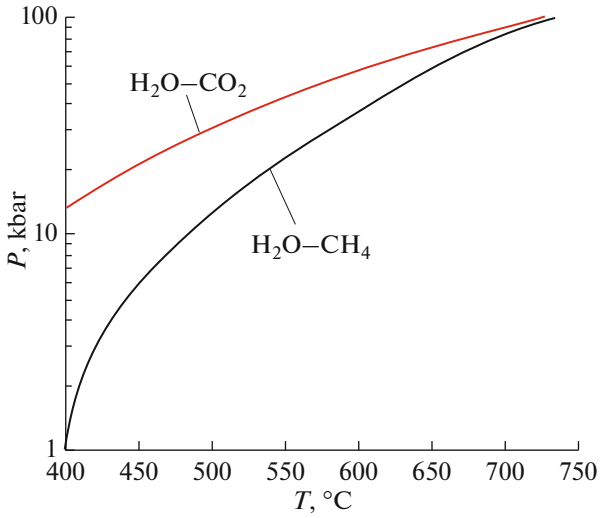

Fig. 4. Minimum pressure values at which the splitting of binary fluids $H_2O–CO_2$ and $H_2O–CH_4$ into coexisting immiscible phases occurs.

the conditions of the cold subduction (Aranovich, 2013).

Our approach allows calculating numerous thermodynamic quantities related to the $H_2O–CO_2–CH_4$ system, in particular, such important quantities as the density and compressibility of fluids. An example of calculation of the density of coexisting immiscible fluid phases at $T = 400°C$ and $P = 4$ kbar is given in Fig. 5. In Figure 5a we present the dependence of the molar volume of fluid on the activity of water on the solvus. This dependence consists of two branches converging at the activity value corresponding to the critical point $a_{H_2O} = a^{crit}_{H_2O}$. Each value of a_{H_2O} greater than $a^{crit}_{H_2O}$ corresponds to two values of the molar volumes of coexisting fluid phases of different compositions. The same compositions of immiscible phases and their molar volumes are retained at a given water activity in the entire region of the heterogeneous fluid. The molar volumes and compositions of the phases make it possible to calculate densities of phases. The corresponding dependence is shown in Fig. 5b. On the right side of the figure, the branches of the curve diverge a considerable distance. High density corresponding to the upper branch of the curve Fig. 5b (it corresponds to a part of the solvus below the position of the critical point in Fig. 1) is due to the lower content of less dense and having low molecular weight methane. This upper branch of the curve Fig. 5b corresponds to the lower branch of the curve Fig. 5a. The compressibility of fluid phases can be obtained by numerical differentiating the molar volumes of the phases obtained at different pressures.

DISCUSSION

The thermodynamics of the $H_2O–CO_2–CH_4$ system was investigated in early works (Kerrick and Jacobs, 1981; Jacobs and Kerrick, 1981) using the HSMRK equation (hard-sphere Redlich-Kwong equation) developed by the authors of these works for H_2O, CO_2, $H_2O–CO_2$, and, separately, for CH_4. The study of activities of H_2O and CO_2 at $T = 400°C$, $P = 25$ kbar, and $x_{CH_4} = 0$ carried out by Jacobs and Kerrick (1981) demonstrates a rather narrow immiscibility gap comparing to that for $T = 400°C$ and $P = 20$ kbar in Fig. 1. This gap obtained in (Jacobs and Kerrick, 1981) disappears when the concentration of methane increases upto $x_{CH_4} = 0.05$. A significant disagreement between the model (Kerrick and Jacobs, 1981;

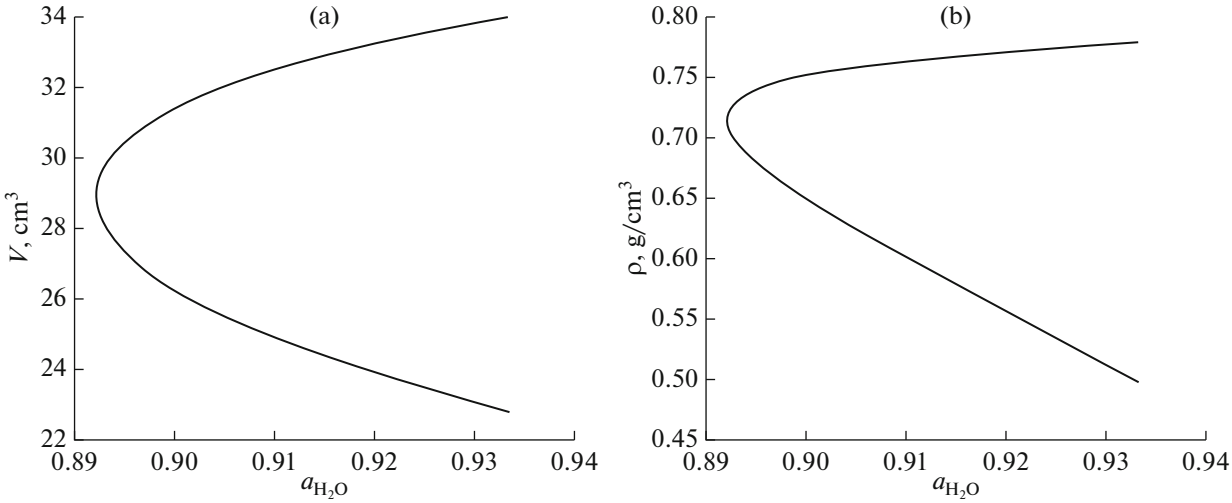

Fig. 5. (a) Molar volumes and (b) densities of coexisting immiscible fluid phases at $T = 400°C$ and $P = 4$ kbar dependent on the chemical activity of water.

Jacobs and Kerrick, 1981) and experimental data for $H_2O–CO_2$ was shown in (Zhang and Duan, 2009). The effect of methane concentration on the character of miscibility in the $H_2O–CO_2–CH_4$ system, opposite to our results, can be explained by the absence of a reliable miscibility model for the $H_2O–CH_4$ subsystem based on experimental results or trustworthy calculations in the HSMRK equation. The work (Plyasunov, 2015) contains a comparative evaluation of a number of equations of state for water-nonpolar gas systems, including equations (Kerrick and Jacobs, 1981; Jacobs and Kerrick, 1981), with a conclusion about the advantages of equations by (Churakov and Gottshalk, 2003a, 2003b; Duan and Zhang, 2006). The equation of state obtained in the last work is an earlier version of the equation we used (Zhang and Duan, 2009).

Thermodynamic behavior of the fluid system $H_2O–CO_2–CH_4$ at *P-T* conditions below the critical point of water was studied in (Zhao, 2017). The picture of the splitting of the fluid into two immiscible phases and behavior of tie lines in the two-phase region have a major similarity with our results shown in Figs. 1–3.

In this work, we studied the phase state and other thermodynamic parameters of the system C–O–H in an assumption that this system consists of molecules H_2O, CO_2, and CH_4 and there are no chemical reactions in the system. These reactions, leading, for example, to appearance of solid carbon or new gaseous particles, like hydrogen, make the thermodynamic behavior of the system more complicated. The influence of the chemical reactions onto phase relations considered in the current work requires a separate study.

The results of our research, presented in Figs. 1–3 show a rather complex behavior of the $H_2O–CO_2–CH_4$ system, which does not quite obviously follow from the known behavior of the $H_2O–CH_4$ and $H_2O–CO_2$ binary systems. The thermodynamic behavior of the $H_2O–CO_2–CH_4$ fluid studied above in the range of *P-T* conditions shown in Figs. 1–3 is of interest from several points of view.

The fluids with high CH_4 and CO_2 contents in the temperature range 400–500°C, along with lower temperatures, are typical for the hydrothermal ore formation processes (Mironova et al., 2018). Due to the presence of salts in ore-forming fluids, the splitting of the fluids into immiscible phases with contrast physical-chemical properties (like shown in Fig. 1 at P = 10–20 kbar), which is favorable for ore deposit formation, can take place at significantly lower pressures, than in the salt-free system, studied above.

Areas of cold subduction, in which the splitting of the $H_2O–CO_2–CH_4$ fluids at temperatures above 500°C is possible, are also a subject of intensive research. At high pressures and the relatively low temperatures considered, the $H_2O–CO_2–CH_4$ system situates in the region of the thermodynamic stability of diamond. In (Frezzotti et al., 2014; Frezzotti, 2019), the formation of micro- and nano-diamonds in cold subduction zones associated with the subduction of the oceanic crust with temperatures not exceeded 600°C to depths of more than 100 km ($P \geq 32$ kbar) was investigated. Reviews of diamond formation during cold subduction are available in (Frezzotti and Ferrando, 2015; Simakov, 2018).

It is of scientific interest to carry out studies similar to that presented above for other gases containing in the fluid. At present, such a study can be facilitated by the presence of a model, similar to used by us, for the $H_2O–H_2$ fluid system (Liu and Cao, 2020).

CONCLUSIONS

In this work, calculations of the thermodynamic properties of the ternary fluid system $H_2O–CO_2–CH_4$ in a broad range of *P-T* parameters above the critical point of water are present. The calculations are based on the known equations of state for binary systems $H_2O–CO_2$ and $H_2O–CH_4$ by (Zhang and Duan, 2009), which were extended up to equation of state of the ternary system by means of the Lorentz–Berthelot mixing rules. The obtained equation for the Gibbs excess free energy allows determining the phase state of the system (homogeneous of two-phase fluid) and obtaining chemical activities of components, densities and compressibility of fluid phases, as well as other thermodynamic properties of the fluid. The equations and methods of calculations can be applied in the range of *P-T* parameters of P = 0.1–100 kbar and T = 400–2300°C, i.e. in the range from metamorphic processes of the greenschist facie up to deep layers of the lithosphere mantle. We obtained phase diagrams of the system $H_2O–CO_2–CH_4$ and investigated dependencies of the chemical activity of water on concentrations of the components and temperature and pressure. The conditions for splitting of the fluid into co-existing immiscible phases are investigated in detail. The splitting in the system $H_2O–CO_2–CH_4$ appears to be possible in the temperature range from 400 up to 735°C. In the range of temperatures 400–480°C and pressures 1.1–10 kbar broad fields of co-existing phases are present on phase diagrams. For the three binary boundary subsystems, the splitting at these *P-T* conditions is possible only in the system $H_2O–CH_4$. Nevertheless, the presence of methane in the ternary system enables the emergence of immiscible fluid phases with high concentration of CO_2, which could exceed the concentration of the methane. At temperatures above 500°C the phase behavior of the system $H_2O–CO_2–CH_4$ is similar to the behavior of the majority of salt-free gas-water fluids, i.e. the splitting into two immiscible phases occurs at high pressures, corresponding to *P-T* conditions of the cold subduction.

A computational program, which implements calculations of the thermodynamic properties of the fluid system $H_2O–CO_2–CH_4$, presented in this work, is available at https://doi.org/10.13140/RG.2.2.16519.32162.

APPENDIX

A known formula (Churakov and Gottschalk, 2003a; Prausnitz et al., 1999):

$$\frac{A^{res}}{RT} = \int_0^{\rho} \frac{Z(\rho, T, x_i) - 1}{\rho} d\rho, \quad \text{(A1)}$$

which connects the compressibility coefficient, molar density $\rho = 1/V$, and molar residual Helmholtz free energy A^{res}, allows obtaining an expression for A^{res} corresponding to the equation of state (1). After replacing ρ to V in Eq. (A1), substitution Eq. (1) for Z, and integration over V, we obtain:

$$\begin{aligned}\frac{A^{res}}{RT} &= \frac{a_1 + a_2/T_m^2 + a_3/T_m^3}{V_m} \\ &+ \frac{a_4 + a_5/T_m^2 + a_6/T_m^3}{2V_m^2} + \frac{a_7 + a_8/T_m^2 + a_9/T_m^3}{4V_m^4} \\ &+ \frac{a_{10} + a_{11}/T_m^2 + a_{12}/T_m^3}{5V_m^5} - \frac{a_{13}}{2a_{15}T_m^3}\left(a_{14} + \frac{a_{15}}{V_m^2} + 1\right) \\ &\times \exp\left(-\frac{a_{15}}{V_m^2}\right) + \frac{a_{13}(a_{14}+1)}{2a_{15}T_m^3}.\end{aligned} \quad \text{(A2)}$$

The last term in this formula does not depend on V_m and provides convergence of A^{res} to zero when infinite increasing the molar volume, i.e. at infinite decreasing density of the fluid. Eq. (A2) for the molar residual Helmholtz free energy allows obtaining equations for the chemical activity of components, their fugacity and fugacity coefficient.

According (Prausnitz et al., 1999), the logarithm of the fugacity coefficient φ_i can be obtained from the formula:

$$\ln \varphi_i = \left[\frac{\partial[n_T A^{res}/(RT)]}{\partial n_i}\right]_{\rho, T, n_{j\neq i}} + (Z-1) - \ln Z, \quad \text{(A3)}$$

where n_T is the total number of moles, and n_i is the number of moles of the component i. Passing from the number of moles to molar fractions and taking into account that, according to formula (A2), $A^{res}/(RT)$ is a function of the quantities T_m and V_m, and that

$$\frac{\partial\left[A^{res}/(RT)\right]}{\partial x_i} = \frac{\partial\left[A^{res}/(RT)\right]}{\partial T_m}\frac{\partial T_m}{\partial x_i} + \frac{\partial\left[A^{res}/(RT)\right]}{\partial V_m}\frac{\partial V_m}{\partial x_i},$$

$$\frac{\partial T_m}{\partial x_i} = -2T_m \frac{\sum_{j=1}^{n} x_j k_{2,ij}\sqrt{\varepsilon_i \varepsilon_j}}{\varepsilon} \text{ and}$$

$$\frac{\partial V_m}{\partial x_i} = -6V_m \frac{\sum_{j=1}^{n} x_j k_{2,ij}(\sigma_i + \sigma_j)/2}{\sigma},$$

we obtain an expression for the logarithm of the fugacity coefficient in the form:

$$\begin{aligned}\ln \varphi_i &= Z - 1 - \ln Z \\ &+ \frac{A^{res}}{RT} - 2S_2\left(1 - \frac{\sum_j k_{1,ij} x_j \sqrt{\varepsilon_i \varepsilon_j}}{\varepsilon}\right) \\ &+ 6(1-Z)\left[1 - \frac{\sum_j k_{2,ij} x_j (\sigma_i + \sigma_j)/2}{\sigma}\right],\end{aligned} \quad \text{(A4)}$$

$$\begin{aligned}S_2 &= \frac{2a_2/T_m^2 + 3a_3/T_m^3}{V_m} + \frac{2a_5/T_m^2 + 3a_6/T_m^3}{2V_m^2} \\ &+ \frac{2a_8/T_m^2 + 3a_9/T_m^3}{4V_m^4} + \frac{2a_{11}/T_m^2 + 3a_{12}/T_m^3}{5V_m^5} \\ &- \frac{3a_{13}}{2a_{15}T_m^3}\left(a_{14} + \frac{a_{15}}{V_m^2} + 1\right)\exp\left(-\frac{a_{15}}{V_m^2}\right) + \frac{3a_{13}(a_{14}+1)}{2a_{15}T_m^3}.\end{aligned} \quad \text{(A5)}$$

The activities of the components are related to the fugacity coefficients by a simple formula:

$$a_i = \frac{x_i \varphi_i}{\varphi_i(x_i = 1)}. \quad \text{(A6)}$$

The Gibbs molar free energy of mixing G_{mix}, required to determine the phase state of the system, is also easily obtained from formula (A4). For a phase of n components, this free energy is calculated by the formula:

$$\begin{aligned}G_{mix} &= RT\sum_{i=1}^{n} x_i \ln x_i \\ &+ RT\sum_{i=1}^{n} x_i \{\ln[\varphi_i(x_i)] - \ln[\varphi_i(x_i = 1)]\}.\end{aligned} \quad \text{(A7)}$$

FUNDING

The work was carried out within the framework of the research theme 0132-2021-0002 (FMUW-2021-0002) "Physicochemical evolution of multicomponent fluids in *P-T* conditions of the crust: new thermodynamic models, application to metamorphic and metasomatic petrogenesis" of the laboratory of fluid processes, IPGG RAS. Computer equipment on which the computing part of the work was performed (graphic computer station) was acquired by IPGG RAS under the program "Updating the instrument base of leading research and development organizations,

academic sector science" within the framework of the national project "Science".

REFERENCES

Aranovich, L.Ya., Fluid–mineral equilibria and thermodynamic mixing properties of fluid systems, *Petrology,* 2013, vol. 21, no. 6, pp. 539–549.

Aranovich, L.Ya., Zakirov, I.V., Sretenskaya, N.G., and Gerya, E.V., Ternary system H_2O–CO_2–NaCl at high *T*–*P* parameters: an empirical mixing model, *Geochem. Int.,* 2010, vol. 48, no. 5, pp. 446–455.

Bushmin, S.A., Vapnik E.A., Ivanov, M.V., et al., Fluids in high-pressure granulites, *Petrology,* 2020, vol. 28, no. 1, pp. 17–46.

Churakov, S.V. and Gottschalk, M., Perturbation theory based equation of state for polar molecular fluids. I. Pure fluids, *Geochim. Cosmochim. Acta,* 2003a, vol. 67, pp. 2397–2414.

Churakov, S.V. and Gottschalk, M., Perturbation theory based equation of state for polar molecular fluids. II. Fluid mixtures, *Geochim. Cosmochim. Acta,* 2003b, vol. 67, pp. 2415–2425.

Duan, Z. and Zhang, Z., Equation of state of the H_2O, CO_2, and H_2O–CO_2 systems up to 10 GPa and 2573.15 K: molecular dynamics simulation with ab initio potential surface, *Geochim. Cosmochim. Acta,* 2006, vol. 70, pp. 2311–2324.

Duan, Z., Møller, N., and Weare, J.H., Equation of state for the NaCl–H_2O–CO_2 system: prediction of phase equilibria and volumetric properties, *Geochim. Cosmochim. Acta,* 1995, vol. 59, pp. 2869–2882.

Fonarev, V.I. and Kreilen, R., Polymetamorphism in the Lapland granulite belt: evidence from fluid inclusions, *Petrology,* 1995, vol. 3, no. 4, pp. 340–356.

Fonarev, V.I., Touret, J.L.R., and Kotelnikova, Z.A., Fluid inclusions in rocks from the Central Kola Granulite area (Baltic Shield), *Eur. J. Mineral.,* 1998, vol. 10, pp. 1181–1200.

Frezzotti, M.L., Diamond growth from organic compounds in hydrous fluids deep within the Earth, *Nature Commun.,* 2019, vol. 10, no. 4952, pp. 1–8.

Frezzotti, M.L. and Ferrando, S., The chemical behavior of fluids released during deep subduction based on fluid inclusions, *Am. Mineral.,* 2015, vol. 100, nos. 2–3, pp. 352–377.

Frezzotti, M.L., Tecce, F., and Casagli, A., Raman spectroscopy for fluid inclusion analysis, *J. Geochem. Explor.,* 2012, vol. 112, pp. 1–20.

Frezzotti, M.L., Huizenga, J.-M., Compagnoni, R., and Selverstone, J., Diamond formation by carbon saturation in C–O–H fluids during cold subduction of oceanic lithosphere, *Geochim. Cosmochim. Acta*, 2014, vol. 143, pp. 68–86.

Ivanov, M.V. and Bushmin, S.A., Equation of state of the H_2O–CO_2–$CaCl_2$ fluid system and properties of fluid phases at *P-T* parameters of the middle and lower crust, *Petrology,* 2019, vol. 27, no. 4, pp. 395–406.

Ivanov, M.V. and Bushmin, S.A., Thermodynamic model of the fluid system H_2O–CO_2–NaCl at *P-T* parameters of the middle and lower crust, *Petrology,* 2021, vol. 29, no. 1, pp. 77–88.

Jacobs, G.K. and Kerrick, D.M., Methane: an equation of state with application to the ternary system H_2O–CO_2–CH_4, *Geochim. Cosmochim. Acta,* 1981, vol. 45, pp. 607–614.

Joyce, D.B. and Holloway, J.R., An experimental determination of the thermodynamic properties of H_2O–CO_2–NaCl fluids at high temperatures and pressures, *Geochim. Cosmochim. Acta,* 1993, vol. 57, pp. 733–746.

Kerrick, D.M. and Jacobs, G.K., A modified Redlich-Kwong equation for H_2O, CO_2, and H_2O–CO_2 mixtures at elevated pressures and temperatures, *Am. J. Sci.,* 1981, vol. 281, pp. 735–767.

Liebscher, A., Experimental studies in model fluid systems, *Rev. Mineral. Geochem.,* 2007, vol. 65, no. 1, pp. 15–47.

Liebscher, A. and Heinrich, C.A., Experimental studies in model fluid systems, *Rev. Mineral. Geochem.,* 2007, vol. 65, no. 1, pp. 1–13.

Liu, Y. and Cao, B., Thermodynamic models for H_2O–CO_2–H_2 mixtures in near-critical and supercritical regions of water, *Int. J. Hydrogen Energy,* 2020, vol. 45, pp. 4297–4304.

Manning, C.E., Fluids of the lower crust: deep is different, *Annu. Rev. Earth Planet. Sci.,* 2018, vol. 46, pp. 67–97.

Manning, C.E. and Aranovich, L.Y., Brines at high pressure and temperature: thermodynamic, petrologic and geochemical effects, *Precambrian Res.,* 2014, vol. 253, pp. 6–16.

Mironova O.F., Naumov V.B., Ryzhenko B.N. Composition of volatile components in mineral-hosted fluid inclusions at hydrothermal deposits. Water–rock–gas systems in ore-forming processes, *Geochem. Int.,* 2018, vol. 56, no. 3, pp. 226–233.

Plyasunov, A.V., Correlation and prediction of thermodynamic properties of nonelectrolytes at infinite dilution of water over very wide temperature and pressure ranges (2000 K and 10 GPa), *Geochim. Cosmochim. Acta,* 2015, vol. 168, pp. 236–260.

Prausnitz, J.M., Lichtenthaler, R.N., and Azevedo, E.G., *Molecular Thermodynamics of Fluid-Phase Equilibria,* New York: Prentice Hall, 1999.

Simakov, S.K., Nano- and micron-sized diamond genesis in nature: An overview, *Geosci. Front.,* 2018, vol. 9, pp. 1849–1858.

Zhang, C. and Duan, Z., A model for C–O–H fluid in the Earth's mantle, *Geochim. Cosmochim. Acta,* 2009, vol. 73, pp. 2089–2102.

Zhao, H., Modeling vapor-liquid phase equilibria of methane–water and methane–carbon dioxide–water system at 247 K to 573 K and 0.1 to 150 MPa using PRSV equation of state and Wong–Sandler mixing rule, *Fluid Phase Equilib.,* 2017, vol. 447, pp. 12–26.